Conductance calculations for quantum wires and interfaces: Mode matching and Green's functions

P. A. Khomyakov, G. Brocks,* V. Karpan, M. Zwierzycki, and P. J. Kelly
Computational Materials Science, Faculty of Science and Technology and MESA+ Research Institute, University of Twente, P. O. Box 217, 7500 AE Enschede, The Netherlands
(Received 25 January 2005; published 19 July 2005)

Landauer's formula relates the conductance of a quantum wire or interface to transmission probabilities. Total transmission probabilities are frequently calculated using Green's-function techniques and an expression derived by C. Caroli *et al.* [J. Phys. C **4**, 916 (1971)]. Alternatively, partial transmission probabilities can be calculated from the scattering wave functions that are obtained by matching the wave functions in the scattering region to the Bloch modes of ideal bulk leads. An elegant technique for doing this, formulated by Ando [Phys. Rev. B **44**, 8017 (1991)], is here generalized to any Hamiltonian that can be represented in tight-binding form. A more compact expression for the transmission matrix elements is derived, and it is shown how all the Green's function results can be derived from the mode-matching technique. We illustrate this for a simple model that can be studied analytically, and for an Fe|vacuum|Fe tunnel junction that we study using first-principles calculations.

DOI: 10.1103/PhysRevB.72.035450 PACS number(s): 73.63.−b, 73.40.−c, 73.20.−r, 85.35.−p

I. INTRODUCTION

Since the discovery of giant magnetoresistance in metallic multilayers there has been considerable interest in studying electronic transport in layered materials.[1,2] At the same time, experimental control of the lateral scale has enabled studies of electronic transport in quantum wires of atomic dimensions.[3] Because of the small dimensions involved, the transport properties of both of these systems should be understood on the basis of their atomic structure. This perception has generated a large effort in recent years to calculate the conductance of multilayers and quantum wires from first principles. Several different approaches have been formulated that have a common basis in the Landauer-Büttiker approach or are equivalent to it. In the linear response regime, the conductance $\mathcal{G}$ is expressed as a quantum-mechanical scattering problem[4] and can be simply related to the total transmission probability at the Fermi energy $T(E_F)$, as

$$\mathcal{G} = \frac{e^2}{h} T(E_F). \tag{1}$$

The multilayer or quantum wire is generally considered as a scattering region of finite size, sandwiched between two semi-infinite ballistic wires. Aiming at a materials-specific description, most current approaches treat the electronic structure within the framework of density-functional theory (DFT).[5–14]

Frequently, the conductance is calculated using a Green's function expression derived by Caroli *et al.*[15,16] An alternative technique, suitable for Hamiltonians that can be represented in tight-binding form, has been formulated by Ando.[17] It is based on directly matching the wave function in the scattering region to the Bloch modes of the leads. The latter technique has been applied to conductance calculations at the empirical tight-binding level,[18] as well as on the first- principles DFT level.[8,19–21] The relationship between the mode-matching[17] and Green's-function[15,16,22] approaches is not immediately obvious. Indeed, it was recently stated that Ando's approach is incomplete and does not yield the correct expression for the conductance.[22]

In this paper we demonstrate that the two approaches are completely equivalent. In the Green's-function approach, a small imaginary part must be added to or subtracted from the energy in order to distinguish between the retarded and advanced forms.[5–7,10–14,22] In mode matching, scattering wave functions are calculated that incorporate the retarded or advanced boundary conditions directly. This makes it possible to solve the scattering problem also at real, instead of complex energies. In addition to yielding the total conductance, by focusing on wave functions the contribution of each individual scattering channel can be identified. In particular, we derive a simple, compact expression for the transmission matrix elements [see Eq. (67)].

The paper is organized as follows. In Sec. II the Hamiltonian we will use is introduced. This model allows us to study both quantum wires that are finite in the directions perpendicular to the wire, and systems that are periodic in these directions, such as single interfaces, sandwiches, and multilayers. We will use the single term "quantum wire" to describe both systems. In Secs. III and IV the mode-matching and Green's-function techniques are summarized. The equivalence of the transmission matrices obtained using these two techniques is demonstrated in Sec. V, and the Caroli expression for the conductance is derived from the mode matching expressions. In Sec. VI the two techniques are applied first to a simple analytical model,[23] and then to an Fe|vacuum|Fe tunnel junction using numerical first-principles calculations. The main conclusions are summarized in Sec. VII.

II. HAMILTONIAN

We set up a tight-binding representation of the Hamiltonian. This is not a severe restriction since a first-principles

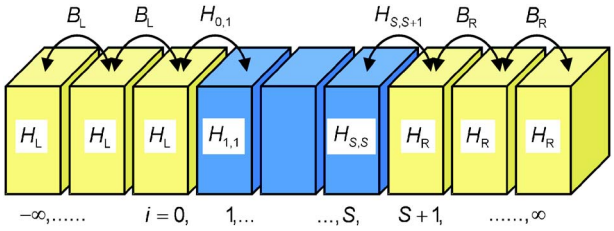

FIG. 1. (Color online) Hamiltonian matrix of a quantum wire divided into slices. The left (L) and right (R) leads are ideal periodic wires that span the cells $i=-\infty,\ldots,0$ and $i=S+1,\ldots,\infty$, respectively. The scattering region spans cells $i=1,\ldots,S$.

DFT implementation that uses a representation on an atomic orbital basis set, has the same mathematical structure as a tight-binding model.[24,25] Alternatively, an implementation that uses a representation of the Hamiltonian on a grid in real space can also be mapped onto a tight-binding model.[26] We begin by dividing the system into slices ("principal layers") perpendicular to the wire direction.[27] The thickness of these slices is chosen such that there is only an interaction between neighboring slices. Labeling each slice with an index i, the Schrödinger equation of the quantum wire becomes

$$-\mathbf{H}_{i,i-1}\mathbf{c}_{i-1}+(E\mathbf{I}-\mathbf{H}_{i,i})\mathbf{c}_i-\mathbf{H}_{i,i+1}\mathbf{c}_{i+1}=0, \tag{2}$$

for $i=-\infty,\ldots,\infty$. Assuming that each slice contains N sites and/or orbitals, $\mathbf{c}_i$ is a vector of dimension N containing the wave-function coefficients on all sites and/or orbitals of slice i. The $N\times N$ matrices $\mathbf{H}_{i,i}$ and $\mathbf{H}_{i,i\pm1}$ consist of, respectively, on-slice and hopping matrix elements of the Hamiltonian, respectively. $\mathbf{I}$ is the $N\times N$ identity matrix. A schematic representation of the structure of the Hamiltonian is given in Fig. 1.

Equation (2) is valid both for quantum wires that are finite in the directions parallel to the slices and for layered systems that are periodic in these directions. In the latter case, translations in the transverse direction can be described in terms of a Bloch wave vector in the two-dimensional Brillouin zone, $\mathbf{k}_\parallel$, which is a good quantum number and the system becomes effectively one dimensional. Explicit expressions for the Hamiltonian matrix elements depend on the particular localized orbital basis or real-space grid representation used.[28] Since details of the tight-binding muffin-tin orbital scheme used in Refs. 8 and 19–21 are given in Ref. 25 and of the real-space high-order finite-difference method can be found in Ref. 26, they will not be discussed further here.

The system is divided into three parts, with $i=-\infty,\ldots,0$ corresponding to the left lead (L), $i=1,\ldots,S$ to the scattering region, and $i=S+1,\ldots,\infty$ to the right lead (R). The leads are assumed to be ideal wires characterized by a periodic potential. It is then sufficient to identify a slice with a translational period along the wire. By construction, the Hamiltonian matrix is the same for each slice of the leads, i.e., $\mathbf{H}_{i,i}\equiv\mathbf{H}_{L/R}$, $\mathbf{H}_{i,i-1}\equiv\mathbf{B}_{L/R}$, and $\mathbf{H}_{i,i+1}\equiv\mathbf{B}_{L/R}^\dagger$ for the left and right leads. Figure 1 summarizes our model of a quantum wire.

III. MODE MATCHING APPROACH

Equation (2) can be solved in a particularly convenient way by a technique that we call mode matching. In this, we follow Ando and generalize his approach to a slice geometry.[17]

A. Bloch matrices

The first step consists of finding solutions for the leads, for which Eq. (2) can be simplified to

$$-\mathbf{B}\mathbf{c}_{i-1}+(E\mathbf{I}-\mathbf{H})\mathbf{c}_i-\mathbf{B}^\dagger\mathbf{c}_{i+1}=0. \tag{3}$$

These equations hold for $i=-\infty,\ldots,-1$ and $i=S+2,\ldots,\infty$, i.e., the left and right leads. To keep the notation as simple as possible, we have omitted the subscripts L and R (see Fig. 1). Since the leads are periodic wires, one can make the ansatz that the solutions have Bloch symmetry, i.e., $\mathbf{c}_i=\lambda\mathbf{c}_{i-1}$, $\mathbf{c}_{i+1}=\lambda^2\mathbf{c}_{i-1}$, where λ is the Bloch factor. Substituting this into Eq. (3) results in a quadratic eigenvalue equation of dimension N. The latter can be solved most easily by transforming it to an equivalent linear (generalized) eigenvalue problem of dimension $2N$ and solving this by a standard algorithm.[29,30]

It can be shown that the equation generally has $2N$ solutions, which can be divided into N right-going modes and N left-going modes,[31] labeled as $(+)$ and $(-)$ in the following. Right-going modes are either evanescent waves that are decaying to the right or waves of constant amplitude that are propagating to the right, whereas left-going modes are decaying or propagating to the left. We denote the eigenvalues by $\lambda_n(\pm)$ where $n=1,\ldots,N$, the corresponding eigenvectors by $\mathbf{u}_n(\pm)$ and write the eigenvalue equation as

$$-\mathbf{B}\mathbf{u}_n(\pm)+(E\mathbf{I}-\mathbf{H})\lambda_n(\pm)\mathbf{u}_n(\pm)-\mathbf{B}^\dagger\lambda_n(\pm)^2\mathbf{u}_n(\pm)=0. \tag{4}$$

In the following we assume that the vectors $\mathbf{u}_n(\pm)$ are normalized; note that, in general, they are *not* orthogonal.

One can distinguish right- from left-going evanescent modes on the basis of their eigenvalues; right-going evanescent modes have $|\lambda(+)|<1$ and left-going evanescent modes have $|\lambda(-)|>1$. Propagating modes have $|\lambda(\pm)|=1$, so here one has to determine the Bloch velocity and use its sign to distinguish right from left propagation. The Bloch velocities are given by the expression

$$v_n(\pm)=-\frac{2a}{\hbar}\,\mathrm{Im}[\lambda_n(\pm)\mathbf{u}_n(\pm)^\dagger\mathbf{B}^\dagger\mathbf{u}_n(\pm)], \tag{5}$$

where a is the slice thickness. A derivation of this equation is given in Appendix A.

Since the eigenvectors are nonorthogonal, it is convenient to define dual vectors $\tilde{\mathbf{u}}_n(\pm)$

$$\tilde{\mathbf{u}}_n^\dagger(\pm)\mathbf{u}_m(\pm)=\delta_{n,m}\quad;\quad\mathbf{u}_n^\dagger(\pm)\tilde{\mathbf{u}}_m(\pm)=\delta_{n,m}. \tag{6}$$

Any wave function in the leads can be expressed as a linear combination of the lead modes. This can be done in a compact form using the two $N\times N$ *Bloch matrices* for right- and left-going solutions

$$\mathbf{F}(\pm) = \sum_{n=1}^{N} \lambda_n(\pm)\mathbf{u}_n(\pm)\tilde{\mathbf{u}}_n^{\dagger}(\pm). \quad (7)$$

For any integer i, $\mathbf{F}^i$ is given by a similar expression but with λ_n replaced by λ_n^i. From the foregoing it is easy to show that the Bloch matrices obey the equation

$$-\mathbf{B}\mathbf{F}^{-1}(\pm) + (E\mathbf{I} - \mathbf{H}) - \mathbf{B}^{\dagger}\mathbf{F}(\pm) = 0. \quad (8)$$

A general solution in the leads can be expressed in terms of a recursion relation

$$\mathbf{c}_i = \mathbf{c}_i(+) + \mathbf{c}_i(-) = \mathbf{F}^{i-j}(+)\mathbf{c}_j(+) + \mathbf{F}^{i-j}(-)\mathbf{c}_j(-). \quad (9)$$

Fixing the coefficients in one slice then sets the boundary conditions and determines the solution for the whole lead.

B. Transmission matrix

The scattering region is defined by $i=1,\ldots,S$ (see Fig. 1). Right and left of the scattering regions one has the recursion relations for the states in the leads from Eq. (9)

$$\begin{aligned}\mathbf{c}_{-1} &= \mathbf{F}_L^{-1}(+)\mathbf{c}_0(+) + \mathbf{F}_L^{-1}(-)\mathbf{c}_0(-) \\ &= [\mathbf{F}_L^{-1}(+) - \mathbf{F}_L^{-1}(-)]\mathbf{c}_0(+) + \mathbf{F}_L^{-1}(-)\mathbf{c}_0, \end{aligned} \quad (10)$$

with $\mathbf{c}_0 = \mathbf{c}_0(+) + \mathbf{c}_0(-)$ and

$$\mathbf{c}_{S+2} = \mathbf{F}_R(+)\mathbf{c}_{S+1}(+) + \mathbf{F}_R(-)\mathbf{c}_{S+1}(-), \quad (11)$$

where the subscripts L and R distinguish between the Bloch matrices of the left and right leads.

The boundary conditions for the scattering problem are set up in the usual way. The vector $\mathbf{c}_0(+)$ is treated as the source, i.e., as a fixed incoming wave from the left lead. There is no incoming wave from the right lead, so we set $\mathbf{c}_{S+1}(-)=0$.

Having set the boundary conditions, Eqs. (10) and (11) can be used to rewrite Eq. (2) in the region not covered by Eq. (3), i.e., for $i=0,\ldots,S+1$. This describes the wave function in the scattering region and the matching to the solutions in the leads. Equation (2) in this region is rewritten as

$$-\mathbf{H}'_{i,i-1}\mathbf{c}_{i-1} + (E\mathbf{I} - \mathbf{H}'_{i,i})\mathbf{c}_i - \mathbf{H}'_{i,i+1}\mathbf{c}_{i+1} = \mathbf{Q}_i\mathbf{c}_0(+), \quad (12)$$

with a modified Hamiltonian matrix defined so $\mathbf{H}'_{i,j} = \mathbf{H}_{i,j}$ for the elements $\{i,j=0,1\}$, $\{i=1,\ldots,S; j=i,i\pm1\}$ and $\{i,j=S+1,S\}$, but with

$$\mathbf{H}'_{0,0} = \mathbf{H}_L + \mathbf{B}_L\mathbf{F}_L^{-1}(-),$$

$$\mathbf{H}'_{S+1,S+1} = \mathbf{H}_R + \mathbf{B}_R^{\dagger}\mathbf{F}_R(+). \quad (13)$$

$\mathbf{H}'_{0,-1}=0$ and $\mathbf{H}'_{S+1,S+2}=0$, so the modified scattering region is decoupled from the leads. On the right-hand side of Eq. (12), we have a source term with

$$\mathbf{Q}_0 = \mathbf{B}_L\,[\mathbf{F}_L^{-1}(+) - \mathbf{F}_L^{-1}(-)], \quad (14)$$

and $\mathbf{Q}_i=0$ for $i=1,\ldots,S+1$. Equation (12) defines a set of $(S+2)\times N$ linear equations. Because the Hamilton matrix is block tridiagonal, each block being of dimension N, this set of equations can be solved efficiently using a block Gaussian elimination scheme.[30] The total wave function $\mathbf{c}_i$ can then be obtained by back substitution.

The transmission is obtained from the wave function in the right lead $\mathbf{c}_{S+1}(+)$. In particular, choosing the incoming wave as one of the modes of the left lead, i.e., $\mathbf{c}_0(+) = \mathbf{u}_{L,m}(+)$, generalized transmission matrix elements $\tau_{n,m}$ are defined by expanding $\mathbf{c}_{S+1}(+)$ in modes of the right lead

$$\mathbf{c}_{S+1}(+) = \sum_{n=1}^{N} \mathbf{u}_{R,n}(+)\tau_{n,m}. \quad (15)$$

By letting $\mathbf{c}_0(+)$ run over all possible incoming modes of the left lead $\mathbf{u}_{L,m}(+)$; $m=1,\ldots,N$, a full-transmission matrix is obtained.

Matrix elements can be defined for all modes, propagating and evanescent, but of course only matrix elements where n,m denote propagating modes contribute to the real physical transmission. These modes can be selected by making use of their eigenvalues; see the discussion following Eq. (4). The physical transmission matrix elements are then found by normalizing with respect to the current[16]

$$t_{n,m} = \sqrt{\frac{v_{R,n}(+)a_L}{v_{L,m}(+)a_R}}\tau_{n,m}, \quad (16)$$

where $v_{L,m}(+)$ and $v_{R,n}(+)$ are the Bloch velocities in the direction of the wire for the right-propagating modes m and n in the left and right leads, respectively [see Eq. (5)]; a_L and a_R are the slice thicknesses of left and right leads.[32] The total transmission probability is given by

$$T(E) = \sum_{n,m}^{(+)} |t_{n,m}|^2, \quad (17)$$

and the conductance is given by Eq. (1) evaluated at $E=E_F$.

C. Green's-function matrix

Solving the set of linear equations, Eq. (12) directly leads to the conductance. However, to facilitate a connection to the Green's-function approach discussed in Sec. IV, we can formulate the solution in a slightly different way. A finite Green's-function matrix $\mathbf{G}'_{i,j}(z), i,j=0,\ldots,S+1$ can be defined by

$$-\mathbf{H}'_{i,i-1}\mathbf{G}'_{i-1,j} + (z\mathbf{I} - \mathbf{H}'_{i,i})\mathbf{G}'_{i,j} - \mathbf{H}'_{i,i+1}\mathbf{G}'_{i+1,j} = \mathbf{I}\delta_{i,j}, \quad (18)$$

with z complex. Note, however, that the matrices $\mathbf{H}'_{0,0}$ and $\mathbf{H}'_{S+1,S+1}$ are non-Hermitian and $\mathbf{G}'_{i,j}(E)$ is also uniquely defined for real energies. The Green's-function matrix allows the solution of Eq. (12) to be written as

$$\mathbf{c}_i = \mathbf{G}'_{i,0}(E)\mathbf{Q}_0\mathbf{c}_0(+). \quad (19)$$

As before, the transmission can be extracted at $i=S+1$ and comparison with Eq. (15) gives

$$\tau_{n,m} = \tilde{\mathbf{u}}_{R,n}^{\dagger}(+)\mathbf{G}'_{S+1,0}(E)\mathbf{Q}_0\mathbf{u}_{L,m}(+), \quad (20)$$

which can be used in Eq. (16). The Green's-function matrix block $\mathbf{G}'_{S+1,0}(E)$ can be found[25] by solving Eq. (18) using a recursive algorithm that resembles a Gaussian elimination scheme.[33]

IV. GREEN's-FUNCTION APPROACH

An apparently quite different route to the transmission matrix starts by defining an infinite Green's-function matrix $\mathbf{G}_{i,j}(z)$ for $i,j=-\infty,\ldots,\infty$ with respect to the original Hamiltonian of Eq. (2).

$$-\mathbf{H}_{i,i-1}\mathbf{G}_{i-1,j}+(z\mathbf{I}-\mathbf{H}_{i,i})\mathbf{G}_{i,j}-\mathbf{H}_{i,i+1}\mathbf{G}_{i+1,j}=\mathbf{I}\delta_{i,j}. \quad (21)$$

Choosing $z=\lim_{\eta\to 0}(E\pm i\eta)$ defines as usual the retarded/advanced Green's-function matrix. We shall use $\mathbf{G}_{i,j}(E)$ to denote the *retarded* Green's-function matrix and $\mathbf{G}^{a}_{i,j}(E)$ to denote the *advanced* Green's-function matrix.

A. Partitioning

Equation (21) is most conveniently solved by applying a partitioning technique.[16,34] It is straightforward to show that the finite part $\mathbf{G}_{i,j}(z)$ defined for $i,j=0,\ldots,S+1$ can be derived from a closed set of equations, similar to Eq. (21), but with $\mathbf{H}_{i,j}$ replaced by $\mathbf{H}''_{i,j}$, where $\mathbf{H}''_{i,j}=\mathbf{H}_{i,j}$ for the elements $\{i,j=0,1\}$, $\{i=1,\ldots,S;j=i,i\pm 1\}$, and $\{i,j=S+1,S\}$, but with

$$\mathbf{H}''_{0,0}(z)=\mathbf{H}_L+\mathbf{B}_L\mathbf{g}_L(z)\mathbf{B}_L^{\dagger},$$

$$\mathbf{H}''_{S+1,S+1}(z)=\mathbf{H}_R+\mathbf{B}_R^{\dagger}\mathbf{g}_R(z)\mathbf{B}_R. \quad (22)$$

Here $\mathbf{g}_L(z)$ and $\mathbf{g}_R(z)$ are the surface Green's functions of the semi-infinite left and right leads, respectively, which can be calculated using an iterative technique. Denoting $\mathbf{G}^{[n]}_{i,j}(z)$ as the solution of an equation similar to Eq. (21), but with $\mathbf{H}_{i,j}=0$ for $\{i>n\vee j>n\}$, one can easily derive the right-going recursion relation

$$[z\mathbf{I}-\mathbf{H}_{n+1,n+1}-\mathbf{H}_{n+1,n}\mathbf{G}^{[n]}_{n,n}(z)\mathbf{H}_{n,n+1}]\mathbf{G}^{[n+1]}_{n+1,n+1}(z)=\mathbf{I}. \quad (23)$$

For an ideal wire with $i,j=-\infty,\ldots,n$, $\mathbf{G}^{[n]}_{n,n}(z)=\mathbf{g}_L(z)$ should be independent of n resulting in the following equation for the surface Green's function,

$$[z\mathbf{I}-\mathbf{H}_L-\mathbf{B}_L\mathbf{g}_L(z)\mathbf{B}_L^{\dagger}]\mathbf{g}_L(z)=\mathbf{I}. \quad (24)$$

Several iterative algorithms have been formulated for solving this nonlinear matrix equation.[27,35,36] A similar reasoning based on a left-going recursion for the right lead results in an equation for the surface Green's function $\mathbf{g}_R(z)$ of the right lead

$$[z\mathbf{I}-\mathbf{H}_R-\mathbf{B}_R^{\dagger}\mathbf{g}_R(z)\mathbf{B}_R]\mathbf{g}_R(z)=\mathbf{I}. \quad (25)$$

Again, setting $z=E+i\eta$ in Eqs. (24) and (25) defines the usual retarded surface Green's functions $\mathbf{g}_{L/R}(E)$. Although we are mainly interested in the physical limit $\lim_{\eta\to 0}$, in practice a finite value of η is often used in order to make the iterative algorithms stable.

The quantities

$$\mathbf{\Sigma}_L(E)=\mathbf{B}_L\mathbf{g}_L(E)\mathbf{B}_L^{\dagger} \quad ; \quad \mathbf{\Sigma}_R(E)=\mathbf{B}_R^{\dagger}\mathbf{g}_R(E)\mathbf{B}_R, \quad (26)$$

which appear in Eqs. (22)–(25), are called the self-energies of the left and right leads, respectively.[16] Once these are obtained, the finite Hamiltonian matrix of Eq. (22) is constructed and the retarded Green's-function matrix $\mathbf{G}_{i,j}(E)$ can be found using a recursive algorithm.[33] Using the lead modes the transmission matrix elements can then be calculated, as will be shown in Sec. IV B. Alternatively, the total transmission probability can be expressed in a form that does not require the lead modes explicitly, which is discussed in Sec. V.

B. Transmission matrix

The transmission matrix can be obtained from the Green's-function matrix of Eq. (21). To do this, we adapt a Fisher-Lee type of approach to our tight-binding formulation.[37] Assuming that the unperturbed reference wave function is the Bloch mode $\mathbf{u}_{L,m}(+)$ that comes in from the left lead, the Lippmann-Schwinger equation[38] in tight-binding form is

$$\mathbf{c}_i=\mathbf{u}_{L,m,i}(+)+\sum_{j,k}\mathbf{G}_{i,j}\mathbf{V}_{j,k}\mathbf{u}_{L,m,k}(+)$$
$$=\left[\mathbf{F}^i_L(+)+\sum_{j,k}\mathbf{G}_{i,j}\mathbf{V}_{j,k}\mathbf{F}^k_L(+)\right]\mathbf{u}_{L,m}(+). \quad (27)$$

Here $\mathbf{u}_{L,m,i}(+)$ is the reference wave function in slice i. It obeys Bloch symmetry and $\mathbf{u}_{L,m}(+)\equiv\mathbf{u}_{L,m,0}(+)$ is the Bloch mode at the origin (see Sec. III A). The matrix $\mathbf{V}_{j,k}$ represents the perturbation with respect to the ideal left lead.

Equation (27) can be simplified using the Dyson equation, which in tight-binding form reads

$$\mathbf{G}_{i,0}=\mathbf{G}^{(0)}_{i,0}+\sum_{j,k}\mathbf{G}_{i,j}\mathbf{V}_{j,k}\mathbf{G}^{(0)}_{k,0}$$
$$=\left[\mathbf{F}^i_L(+)+\sum_{j,k}\mathbf{G}_{i,j}\mathbf{V}_{j,k}\mathbf{F}^k_L(+)\right]\mathbf{G}^{(0)}_{0,0}, \quad (28)$$

using Eq. (32). Comparing Eqs. (27) and (28) one finds the simple expression

$$\mathbf{c}_i=\mathbf{G}_{i,0}(E)[\mathbf{G}^{(0)}_{0,0}(E)]^{-1}\mathbf{u}_{L,m}(+). \quad (29)$$

From the definition of the generalized transmission matrix elements, cf. Eq. (15), one then obtains the expression

$$\tau_{n,m}=\tilde{\mathbf{u}}^{\dagger}_{R,n}(+)\mathbf{G}_{S+1,0}(E)[\mathbf{G}^{(0)}_{0,0}(E)]^{-1}\mathbf{u}_{L,m}(+). \quad (30)$$

To find $\tau_{n,m}$ one needs to calculate only the Green function matrix blocks $\mathbf{G}_{S+1,0}(E)$ of the full system and $\mathbf{G}^{(0)}_{0,0}(E)$ of the ideal left lead. The physical transmission matrix elements and the total transmission probability can then be obtained from Eqs. (16) and (17).

V. MODE MATCHING VERSUS GREEN's FUNCTIONS

The two seemingly different formalisms introduced in Secs. III and IV are, in fact, closely related. In this section we will show how all Green's-function results can be obtained from the mode-matching approach. We begin by expressing the Green's-function matrices of ideal wires in terms of the Bloch matrices, $\mathbf{F}(\pm)$. These expressions are then used to prove that the transmission matrix elements ob-

tained from the mode-matching and Green's-function approaches [cf. Eqs. (20) and (30)] are, in fact, identical. After that, we show that the transmission matrix elements are independent of the exact positions within the leads that are used to match the leads to the scattering region, apart from a trivial phase factor. Then we derive from the mode-matching expression for the total transmission probability the Green's-function expression known as the Caroli expression.[15] Finally, a more compact expression for the transmission matrix elements is derived.

A. Green's functions of ideal wires in terms of Bloch matrices

We begin by deriving an expression for the retarded Green's-function matrix $\mathbf{G}^{(0)}_{i,j}$ of an *ideal infinite wire* in terms of its eigenmodes.[39] The columns of such a Green's function obey the equation

$$-\mathbf{B}\mathbf{G}^{(0)}_{i-1,j} + (E^{+}\mathbf{I} - \mathbf{H})\mathbf{G}^{(0)}_{i,j} - \mathbf{B}^{\dagger}\mathbf{G}^{(0)}_{i+1,j} = \mathbf{I}\delta_{i,j}, \tag{31}$$

where $E^{+}=E+i\eta$. For $i\neq j$ the solution is similar to that of the wave functions [see Eq. (3)]. In addition, the retarded Green's function should consist only of propagating waves that move outward from the δ source and/or evanescent states that decay away from the source.[38] From Eq. (9), we have the *column* recursion relations

$$\mathbf{G}^{(0)}_{i,j}(E) = \mathbf{F}^{i-j}(-)\mathbf{G}^{(0)}_{j,j}(E),\ i<j,$$

$$\mathbf{G}^{(0)}_{i,j}(E) = \mathbf{F}^{i-j}(+)\mathbf{G}^{(0)}_{j,j}(E),\ i>j. \tag{32}$$

The diagonal block $\mathbf{G}^{(0)}_{j,j}(E)$ can now be obtained by combining Eqs. (31) and (32), which gives for $i=j$

$$[-\mathbf{B}\mathbf{F}^{-1}(-) + E^{+}\mathbf{I} - \mathbf{H} - \mathbf{B}^{\dagger}\mathbf{F}(+)]\mathbf{G}^{(0)}_{j,j} = \mathbf{I}. \tag{33}$$

Eliminating $E^{+}\mathbf{I}-\mathbf{H}$ using Eq. (8) then yields

$$[\mathbf{G}^{(0)}_{j,j}(E)]^{-1} = \mathbf{B}[\mathbf{F}^{-1}(+) - \mathbf{F}^{-1}(-)], \tag{34}$$

or the equivalent

$$[\mathbf{G}^{(0)}_{j,j}(E)]^{-1} = \mathbf{B}^{\dagger}[\mathbf{F}(-) - \mathbf{F}(+)], \tag{35}$$

Equations (32) and (34) represent the full expression for the Green's function $\mathbf{G}^{(0)}_{i,j}$ of an infinite ideal wire in terms of the Bloch matrices $\mathbf{F}(\pm)$ and thus in terms of the eigenmodes. Note that we can set $E^{+}=E$ since, in terms of the modes, the retarded Green's-function matrix is uniquely defined for real energies.

The *advanced* Green's-function matrix $\mathbf{G}^{(0)a}_{i,j}(E)$ can be found from a similar procedure. It should consist of propagating waves that move toward the source and/or evanescent states that grow toward the source. One can construct two new Bloch matrices $\mathbf{F}^{a}(\pm)$, which are similar to those defined in Eq. (7). In $\mathbf{F}^{a}(+)$ one collects the modes that are decaying to the right (growing to the left) and modes that are propagating to the left. $\mathbf{F}^{a}(-)$ then contains modes that grow or propagate to the right

$$\mathbf{F}^{a}(\pm) = \sum_{n=1}^{N} \lambda^{a}_{n}(\pm)\mathbf{u}^{a}_{n}(\pm)\tilde{\mathbf{u}}^{a\dagger}_{n}(\pm),\ \text{with}$$

$$\lambda^{a}_{n}(\pm) = \lambda_{n}(\mp),\quad \mathbf{u}^{a}_{n}(\pm) = \mathbf{u}_{n}(\mp)\ \text{propagating}$$

$$\lambda^{a}_{n}(\pm) = \lambda_{n}(\pm),\quad \mathbf{u}^{a}_{n}(\pm) = \mathbf{u}_{n}(\pm)\ \text{evanescent}. \tag{36}$$

Using these definitions, expressions for the advanced Green's-function matrix are obtained from Eqs. (32) and (34) by replacing $\mathbf{F}(\pm)$ with $\mathbf{F}^{a}(\pm)$.

From the general relation between retarded and advanced Green's functions, $\mathbf{G}_{i,j}=(\mathbf{G}^{a}_{j,i})^{\dagger}$, the following *row* recursion relations can be deduced for the retarded Green's function

$$\mathbf{G}^{(0)}_{i,j}(E) = \mathbf{G}^{(0)}_{i,i}(E)[\mathbf{F}^{a\dagger}(+)]^{j-i},\ i<j,$$

$$\mathbf{G}^{(0)}_{i,j}(E) = \mathbf{G}^{(0)}_{i,i}(E)[\mathbf{F}^{a\dagger}(-)]^{j-i},\ i>j. \tag{37}$$

The retarded Green's function $\mathbf{G}^{(s)}_{i,0}(E)$ of a *semi-infinite wire* extending from $i=-\infty,\ldots,0$ can be obtained using a similar technique. Instead of Eq. (32), we get

$$\mathbf{G}^{(s)}_{i,0}(E) = \mathbf{F}^{i}(-)\mathbf{g}(E),\ i<0, \tag{38}$$

where $\mathbf{g}(E)=\mathbf{G}^{(s)}_{0,0}(E)$ is the surface Green's function. Using this in Eq. (31) gives for $i=0$ and $j=0$ and for $i=-1$ and $j=0$, respectively,

$$[-\mathbf{B}\mathbf{F}^{-1}(-) + E^{+}\mathbf{I} - \mathbf{H}]\,\mathbf{g} = \mathbf{I},$$

$$[-\mathbf{B}\mathbf{F}^{-1}(-) + E^{+}\mathbf{I} - \mathbf{H}]\,\mathbf{F}^{-1}(-)\mathbf{g} = \mathbf{B}^{\dagger}\mathbf{g}. \tag{39}$$

Note that the $\mathbf{B}^{\dagger}$ term is absent in the first equation since we are dealing with a semi-infinite wire. These two equations can be easily solved to find an expression for the surface Green's-function[27,40,39]

$$\mathbf{g}(E) = \mathbf{F}^{-1}(-)(\mathbf{B}^{\dagger})^{-1}. \tag{40}$$

Equations (38) and (40) represent the Green's function of a semi-infinite ideal wire extending from $i=-\infty,\ldots,0$. In a similar fashion, one gets for the Green's function of a semi-infinite ideal wire extending from $i=0,\ldots,\infty$

$$\mathbf{G}^{(s)}_{i,0}(E) = \mathbf{F}^{i+1}(+)\mathbf{B}^{-1},\ i\geqslant 0. \tag{41}$$

Analogously to Eqs. (38)–(41), one can define the advanced Green's-function matrix $\mathbf{G}^{(s)a}_{i,0}(E)$ in terms of the Bloch matrices $\mathbf{F}^{a}(\pm)$. Moreover, since $[\mathbf{g}^{a}]^{\dagger}=\mathbf{g}$, we have the following relation between the Bloch matrices:

$$\mathbf{B}^{\dagger}\mathbf{F}(\pm) = \mathbf{F}^{a\dagger}(\pm)\mathbf{B}. \tag{42}$$

B. Equivalence of mode-matching and Green's-function approaches

The retarded surface Green's functions of the left and right leads can be derived from Eqs. (40) and (41)

$$\mathbf{g}_L(E) = \mathbf{F}_L^{-1}(-)[\mathbf{B}_L^\dagger]^{-1}; \quad \mathbf{g}_R(E) = \mathbf{F}_R(+)\mathbf{B}_R^{-1}. \tag{43}$$

The retarded self-energies of Eq. (26) are then given by

$$\mathbf{\Sigma}_L(E) = \mathbf{B}_L\mathbf{F}_L^{-1}(-); \quad \mathbf{\Sigma}_R(E) = \mathbf{B}_R^\dagger\mathbf{F}_R(+). \tag{44}$$

Comparing Eqs. (13) and (22) then establishes

$$\mathbf{G}'_{i,j}(E) = \mathbf{G}_{i,j}(E). \tag{45}$$

In other words, the two Green's functions discussed in Secs. III and IV are identical.

By comparing Eqs. (14) and (34) one has

$$\mathbf{Q}_0 = [\mathbf{G}^{(0)}_{0,0}(E)]^{-1}. \tag{46}$$

In conclusion, the two expressions for the generalized transmission matrix elements [Eqs. (20) and (30)] are identical.

C. Invariance of transmission probability

Apart from trivial phase factors, the transmission matrix elements should not depend on where in the ideal lead the wave-function matching is carried out. In a recent paper it was stated that Ando's expression for $t_{n,m}$ [Eqs. (20) and (16)] lacks this invariance property and is therefore incomplete.[22] One can, however, prove directly from Eq. (20) that the transmission matrix elements do have the required invariance property.[41] The proof becomes easier if the equivalence of Eqs. (20) and (30), established above, is used.

The scattering region runs from slices 0 to $S+1$ if we include the boundaries with the left and right leads. This means that the Green's-function matrix $\mathbf{G}_{i,j}$ with indices i,j outside this region obeys the equations for the ideal leads. From the column and row recursion relations [Eqs. (32) and (37)] one derives

$$\mathbf{G}_{S+1+i,j}(E) = \mathbf{F}_R^i(+)\mathbf{G}_{S+1,0}(E)[\mathbf{F}_L^{a\dagger}(-)]^j, \tag{47}$$

for $j<0, i>0$. In a similar way, one derives for the Green's-function matrix of the left lead

$$\mathbf{G}^{(0)}_{j,j}(E) = \mathbf{F}_L^j(+)\mathbf{G}^{(0)}_{0,0}(E)[\mathbf{F}_L^{a\dagger}(-)]^j, \tag{48}$$

for $j<0$.

We now artificially extend the scattering region by including slices from the left and right leads and let it run from $j<0$ to $S+1+i$ with $i>0$. Equation (30) gives for the transmission matrix element

$$\tau'_{n,m} = \tilde{\mathbf{u}}^\dagger_{R,n}(+)\mathbf{G}_{S+1+i,j}(E)[\mathbf{G}^{(0)}_{j,j}(E)]^{-1}\mathbf{u}_{L,m}(+). \tag{49}$$

Using (47) and (48) then gives

$$\begin{aligned}\tau'_{n,m} &= \tilde{\mathbf{u}}^\dagger_{R,n}(+)\mathbf{F}_R^i(+)\mathbf{G}_{S+1,0}(E)[\mathbf{G}^{(0)}_{0,0}(E)]^{-1}\mathbf{F}_L^{-j}(+)\mathbf{u}_{L,m}(+)\\ &= \lambda^i_{R,n}(+)\lambda^{-j}_{L,m}(+)\tau_{n,m} = e^{i\alpha}\tau_{n,m},\end{aligned} \tag{50}$$

with α real. The second equality in Eq. (50) follows from applying Eq. (7). The last equality follows from the fact that we are only interested in propagating states and for propagating states $|\lambda|=1$. Using this result in (16) and (17) proves the invariance of the total transmission probability with respect to moving the boundaries between leads and scattering region into the leads.

D. The Caroli expression

The total transmission probability is given by Eq. (17), where the sum has to be over propagating states only. We can extend the summation to include all N states (propagating and evanescent) by defining an $N\times N$ transmission matrix

$$\mathbf{t} = \mathbf{V}_R^{1/2}(+)\tau\tilde{\mathbf{V}}_L^{1/2}(+), \tag{51}$$

where τ is the matrix whose elements are given by Eq. (20). $\mathbf{V}_R(+)$ is defined as the singular, diagonal matrix that has the velocities $v_{R,n}$ times the constant $\hbar/a_R$ on the diagonal for the right-propagating states and zeros for evanescent states. We call it the velocity matrix. Likewise a pseudoinverse velocity matrix $\tilde{\mathbf{V}}_L(+)$ can be defined, which has $1/v_{L,n}\times a_L/\hbar$ on the diagonal for left-propagating states and all other matrix elements are zero. These velocity matrices project onto the space of the propagating states so that the transmission matrix has only nonzero values between propagating states. Equation (17) can then be expressed in the familiar form

$$T = \mathrm{Tr}[\mathbf{t}^\dagger\mathbf{t}] = \mathrm{Tr}[\tau^\dagger\,\mathbf{V}_R(+)\tau\tilde{\mathbf{V}}_L(+)]. \tag{52}$$

Using the above definition of the velocity matrix and Ando's expressions for the transmission matrix elements, we will show how (52) can be rewritten as

$$T = \mathrm{Tr}[\mathbf{\Gamma}_R\mathbf{G}^r\mathbf{\Gamma}_L\mathbf{G}^a], \tag{53}$$

where $\mathbf{G}^r$, $\mathbf{G}^a$ are short-hand notations for $\mathbf{G}_{S+1,0}(E)$ and $\mathbf{G}^a_{0,S+1}(E)$, respectively. The matrices $\Gamma_{L/R}$ are defined as

$$\mathbf{\Gamma}_{L/R} = i[\mathbf{\Sigma}_{L/R} - \mathbf{\Sigma}^\dagger_{L/R}]. \tag{54}$$

Equation (53) is known as the Caroli expression[15] and often used to calculate transmission probabilities.[16,22] It is equivalent to the Kubo-Greenwood expression for the linear response regime.[14,42] The latter expression is also equivalent to Landauer's formula.[43]

The first step is to construct $N\times N$ matrices $\mathbf{U}(\pm)$, the columns of which are the eigenmodes $\mathbf{u}_n(\pm)$, and diagonal matrices $\Lambda(\pm)$, the elements of which are the eigenvalues $\lambda_n(\pm)$

$$\mathbf{U}(\pm) = (\mathbf{u}_1(\pm)\mathbf{u}_2(\pm)\cdots\mathbf{u}_N(\pm)), \tag{55}$$

$$\mathbf{\Lambda}(\pm)_{m,n} = \lambda_n(\pm)\,\delta_{m,n}. \tag{56}$$

From Eqs. (6) and (9) it is then easy to show that the dual vectors $\tilde{\mathbf{u}}_n(\pm)$ form the columns of the matrix $[\mathbf{U}(\pm)^{-1}]^\dagger$ and that the $\mathbf{F}(\pm)$ matrices obey the equation

$$\mathbf{F}(\pm)\mathbf{U}(\pm) = \mathbf{U}(\pm)\mathbf{\Lambda}(\pm). \tag{57}$$

In a similar way matrices $\mathbf{U}^a(\pm)$ and $\mathbf{\Lambda}^a(\pm)$ can be constructed [see Eq. (36)].

Using these definitions, one can generalize the τ matrix of Eq. (20) to

$$\tau = \mathbf{U}_R^{-1}(+)\mathbf{G}^r\mathbf{Q}_0\mathbf{U}_L(+). \tag{58}$$

Note that τ-matrix elements are defined not only between propagating states, but also between evanescent states. How-

ever, as we remarked above already, only propagating states contribute to the physical transmission.

The second step is to express the velocity matrices in terms of the $\mathbf{\Gamma}$ matrices. To do this we use an expression for the velocity matrix,

$$\mathbf{V}(\pm) = i[\mathbf{U}^\dagger(\pm)\mathbf{B}^\dagger\mathbf{U}(\pm)\mathbf{\Lambda}(\pm) - \mathbf{\Lambda}^\dagger(\pm)\mathbf{U}^\dagger(\pm)\mathbf{B}\mathbf{U}(\pm)], \tag{59}$$

which can be shown (see Appendix A for a proof) to be equivalent to the definition introduced in the first paragraph of this section. Using (57), this can be rewritten for the right lead as

$$\begin{aligned}\mathbf{V}_R(+) &= i\mathbf{U}_R^\dagger(+)[\mathbf{B}_R^\dagger\mathbf{F}_R(+) - \mathbf{F}_R^\dagger(+)\mathbf{B}_R]\mathbf{U}_R(+) \\ &= i\mathbf{U}_R^\dagger(+)[\mathbf{\Sigma}_R - \mathbf{\Sigma}_R^\dagger]\mathbf{U}_R(+) \\ &= \mathbf{U}_R^\dagger(+)\mathbf{\Gamma}_R\mathbf{U}_R(+).\end{aligned} \tag{60}$$

The second line follows from (44). A similar relation between the $\mathbf{\Gamma}$ matrix and the velocity matrix for the left lead can be shown to exist,

$$\mathbf{V}_L(+) = \mathbf{U}_L^{a\dagger}(-)\mathbf{\Gamma}_L\mathbf{U}_L^a(-), \tag{61}$$

by using (42) and an equivalent expression for the velocity matrix [Eq. (A7)]. Equations (60) and (61) imply that the $\mathbf{\Gamma}$ matrices project onto the space spanned by the propagating states.

The third step is to introduce a matrix $\mathbf{P}$ that explicitly projects onto the propagating states of the left lead

$$\mathbf{P} = \mathbf{U}_L(+)\mathbf{I}_p[\mathbf{U}_L^a(-)]^{-1} = \sum_{n=1}^{N_p}\mathbf{u}_{L,n}(+)\tilde{\mathbf{u}}_{L,n}^{a\dagger}(-), \tag{62}$$

where the $\mathbf{I}_p$ matrix contains 1 on the N_p diagonal elements that correspond to propagating states, and 0 at all other positions. Given this projector matrix, it is possible to prove that

$$\mathbf{Q}_0\mathbf{P} = i\mathbf{\Gamma}_L. \tag{63}$$

The proof is given in Appendix B. Using this property one has

$$\begin{aligned}\mathbf{Q}_0\mathbf{U}_L(+)\tilde{\mathbf{V}}_L(+) &= \mathbf{Q}_0\mathbf{P}\mathbf{U}_L^a(-)\tilde{\mathbf{V}}_L(+) = i\mathbf{\Gamma}_L\mathbf{U}_L^a(-)\tilde{\mathbf{V}}_L(+) \\ &= i[\mathbf{U}_L^{a\dagger}(-)]^{-1}\mathbf{V}_L(+)\tilde{\mathbf{V}}_L(+) = i[\mathbf{U}_L^{a\dagger}(-)]^{-1}\mathbf{I}_p.\end{aligned} \tag{64}$$

Substituting (58), (60), and (64) into (52) leads directly to the Caroli expression [Eq. (53)].

E. Transmission matrix: A compact expression

Using the results of the previous section it is possible to derive a more compact expression for the transmission matrix. Combining (51), (58), and (62), one has

$$\mathbf{t} = \mathbf{V}_R^{1/2}(+)\mathbf{U}_R^{-1}(+)\mathbf{G}^r\mathbf{Q}_0\mathbf{P}\mathbf{U}_L^a(-)\tilde{\mathbf{V}}_L^{1/2}(+). \tag{65}$$

By following the same steps as in Eq. (64) and using $\mathbf{V}_L\tilde{\mathbf{V}}_L^{1/2} = \mathbf{V}_L^{1/2}$ this can be simplified to

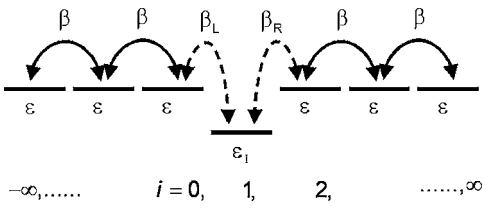

FIG. 2. Parameters of a one-band nearest-neighbor tight-binding model for a single impurity in a one-dimensional chain.

$$\mathbf{t} = i\mathbf{V}_R^{1/2}(+)\mathbf{U}_R^{-1}(+)\mathbf{G}^r[\mathbf{U}_L^{a\dagger}(-)]^{-1}\mathbf{V}_L^{1/2}(+). \tag{66}$$

Writing out the transmission matrix elements gives the compact expression

$$t_{n,m} = i\hbar\sqrt{\frac{v_{R,n}v_{L,m}}{a_R a_L}}\,\tilde{\mathbf{u}}_{R,n}^\dagger(+)\mathbf{G}_{S+1,0}(E)\tilde{\mathbf{u}}_{L,m}^a(-). \tag{67}$$

This is the tight-binding equivalent of the Fisher-Lee expression relating transmission and Green's-function matrices.[37]

VI. EXAMPLES

A. Simple analytical model

We consider a system consisting of a single impurity in a one-dimensional chain and treat this within a one-band nearest-neighbor tight-binding model. The parameters of this model are given in Fig. 2. This model can be solved analytically,[23] so it can serve as a simple test to illustrate the equivalence of the different approaches.

We will first solve the problem using the mode-matching approach of Sec. III. It is convenient to define a scaled energy by

$$\omega \equiv \frac{E-\epsilon}{2\beta}. \tag{68}$$

The model involves only one channel and with $\mathbf{u}_m(\pm) = 1$, Eq. (4) reduces to

$$-\beta + (E-\epsilon)\lambda(\pm) - \beta\lambda(\pm)^2 = 0. \tag{69}$$

The roots $\lambda(\pm)$ can be given a more familiar form. For $|\omega| \leqslant 1$, we define a wave number k by

$$\cos(ka) = \omega, \tag{70}$$

where a is the lattice parameter. From Eqs. (69) and (70) one then obtains

$$\lambda(\pm) = e^{\pm ika}, \tag{71}$$

which describes propagating states. For $|\omega| > 1$ one defines κ by

$$\cosh(\kappa a) = |\omega|. \tag{72}$$

One obtains $\lambda(\pm) = \exp(\mp\kappa a)$ if $\omega > 1$ and $\lambda(\pm) = -\exp(\mp\kappa a)$ if $\omega < -1$; both cases describe evanescent states.

Since the scattering region consists of a single impurity, $S=1$, Eqs. (12)–(14) give three linear equations with three

unknowns describing the scattering problem. In a one-channel model, one has $\mathbf{F}(\pm)=\lambda(\pm)$ and $\lambda(\pm)^{-1}=\lambda(\mp)$. There is only one possible incoming wave, so $\mathbf{c}_0(+)=1$. The linear equations then become in matrix form

$$\mathbf{A}\begin{pmatrix} c_0 \\ c_1 \\ c_2 \end{pmatrix} = \begin{pmatrix} \beta[\lambda(-)-\lambda(+)] \\ 0 \\ 0 \end{pmatrix}, \tag{73}$$

with

$$\mathbf{A} = \begin{pmatrix} E-\epsilon-\beta\lambda(+) & -\beta_L & 0 \\ -\beta_L & E-\epsilon_I & -\beta_R \\ 0 & -\beta_R & E-\epsilon-\beta\lambda(+) \end{pmatrix}. \tag{74}$$

Solving this set of equations and using Eqs. (70) and (71) we obtain the compact expression

$$c_2 = e^{2ika}\frac{-if\sin(ka)}{d+(1-b)\cos(ka)-ib\sin(ka)}, \tag{75}$$

defining the dimensionless parameters

$$b=\frac{\beta_L^2+\beta_R^2}{2\beta^2}, \quad d=\frac{\epsilon-\epsilon_I}{2\beta}, \quad f=\frac{\beta_L\beta_R}{\beta^2}. \tag{76}$$

Applying Eqs. (15)–(17) then yields for the total transmission probability

$$T(E)=|c_2|^2. \tag{77}$$

Using Eqs. (70) and (75) it is easy to show that this transmission probability is identical to Eq. (15) of Ref. 23, which was obtained using a different technique.

It is instructive to solve the same problem using the Green's-function approach of Sec. IV A. First, one has to find the surface Green's functions of the leads from Eqs. (24) and (25), which for the current model become

$$[E-\epsilon-\beta^2 g(E)]g(E)=1, \tag{78}$$

where E is a real energy. This equation has the solutions

$$g^{\pm}(E)=\frac{e^{\pm ika}}{\beta}, \tag{79}$$

for both leads. The Green's-function matrix in the scattering region can then be found from Eqs. (21) and (22), which can be combined in the 3×3 matrix equation

$$\mathbf{A}\mathbf{G}(E)=\mathbf{I}, \tag{80}$$

where $G_{i,j}(E), i,j=0,\ldots,2$ are the matrix elements of $\mathbf{G}(E)$ and $\mathbf{A}$ is given by Eq. (74). Inverting $\mathbf{A}$ yields the matrix element

$$G_{2,0}(E)=\frac{f}{2\beta}\frac{e^{2ika}}{d+(1-b)\cos(ka)-ib\sin(ka)}, \tag{81}$$

with the parameters b, d, and f defined by Eq. (76). The relevant Green's-function matrix element for the ideal lead is found from Eq. (34)

$$G_{0,0}^{(0)}(E)=\frac{i}{2\beta\sin(ka)}. \tag{82}$$

Using these results in Eq. (30) one observes that the expression for the (one-channel) transmission matrix element becomes identical to Eq. (75).

Finally one can calculate the transmission probability from the Caroli expression given in Sec. V D [cf. Eq. (53)]. Using Eqs. (26), (54), and (79) one obtains

$$\Gamma_L=\Gamma_R=-2\beta\sin(ka), \tag{83}$$

for left and right leads. Using Eqs. (81) and (83), and $G_{0,2}^a=(G_{2,0})^*$ in Eq. (53) then yields an expression for the transmission probability that is identical to Eq. (77). It illustrates the equivalence of the different approaches for calculating the transmission in this simple model.

In addition to providing a channel for propagating states, an impurity can also give rise to localized states, whose energy is outside the energy band of the chain [cf. Eq. (72)]. Such a state does not contribute to the physical transmission, but the transmission amplitude has a pole at an energy that corresponds to a localized state.[44] Within the mode-matching approach this corresponds to an energy at which c_{S+1} becomes infinite. For the present model the energies of localized states can be obtained by setting $k=i\kappa$ and setting the denominator to zero in Eq. (75). This leads to

$$(\omega+d)(\omega+\mathrm{sgn}(\omega)\sqrt{\omega^2-1})-b=0; \quad |\omega|>1, \tag{84}$$

the roots of which give the energies of the localized states. Again, these results are equivalent to the results obtained using the approach of Ref. 23.

Within the Green's-function approach the energies of the localized states are given by the poles of the Green's-function matrix. Via Eq. (81) this again leads to Eq. (84). Alternatively, since the Green's function matrix is the inverse of the $\mathbf{A}$ matrix [cf. Eq. (80)], its poles are given by the roots of $\det(\mathbf{A})=0$. This equation is equivalent to Eq. (84), as is easily shown by setting $\lambda(+)=\pm\exp(-\kappa a)$ in the $\mathbf{A}$ matrix.

B. Fe|vacuum|Fe tunnel junction

As an example of a more complex system, we consider an Fe|vacuum|Fe tunnel junction where the electronic structure is treated using the local-density approximation of DFT.[45] The calculations are based on a tight-binding muffin-tin orbital (TB-MTO) atomic spheres approximation (ASA) implementation[8,19–21,25] of the formalism described in Sec. III.

The first step in the calculation is the self-consistent determination of the electronic structure of the tunnel junction using the layer Green's function approach of Ref. 35. The Fe leads are oriented in the (001) direction, and the atoms at the Fe(001) surfaces are kept at their unrelaxed bulk positions. For the bcc structure and TB-MTOs,[46] a principal layer in the (001) direction contains two monolayers of Fe with a thickness of 2.866 Å. The vacuum region is modeled by a number of such slices, of the same thickness, filled with "empty" spheres of the same size and packing as the Fe atomic spheres. The atomic sphere potentials of the vacuum region

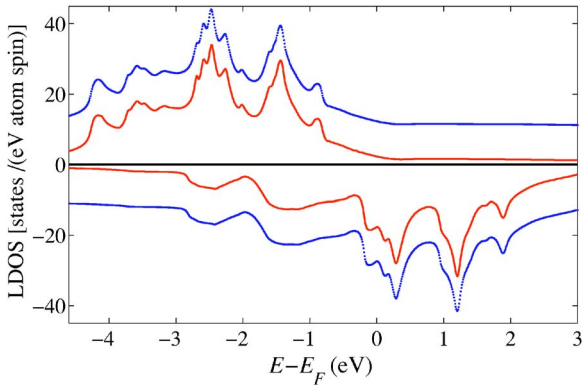

FIG. 3. (Color online) Layer density of states (LDOS) at the Fe(001) surface layer. Top panel: majority spin. Top curve (red, dashed): as calculated using the layer Green's-function method.[35] Bottom curve (blue, solid): as calculated using the mode-matching approach. Both calculations use η=0.0025 Ry. For clarity, the top curve has been displaced by 10 units along the y axis. Bottom panel: minority spin, the LDOS is shown with a negative sign.

and four monolayers (two principal layers) of Fe on either side of the vacuum are calculated self-consistently, while the potentials of more distant layers are kept at their bulk values. These potentials then form the input to a transmission calculation based on mode matching.[8,20,21] Further technical details can be found in Ref. 25.

A useful quantity to extract from the self-consistent layer calculation is the layer density of states (LDOS) $\rho_i(E)$. It is related to the retarded Green's-function matrix defined in Eq. (21) by

$$\rho_i(E+i\eta) = -\pi^{-1}\,\mathrm{Im}\,\mathrm{Tr}[\mathbf{G}_{i,i}(E+i\eta)], \tag{85}$$

where the trace refers to the usual lm angular momentum indices characterizing MTOs. For reasons of numerical stability the retarded Green's-function matrix is calculated by adding a finite imaginary part to the energy; we have used η=0.0025 Ry. In the mode-matching approach, the LDOS can be directly expressed in terms of the wave functions or, alternatively, in terms of the Green's-function matrix of Eq. (18)

$$\rho_i(E) = -\pi^{-1}\,\mathrm{Im}\,\mathrm{Tr}[\mathbf{G}'_{i,i}(E)]. \tag{86}$$

This Green's-function matrix can be calculated for a real energy, but in order to make a comparison to the results obtained with Eq. (85), we add an imaginary part, η =0.0025 Ry.

In Fig. 3 we compare the LDOS obtained using (85) and (86) for the topmost Fe monolayer of (001) Fe|vacuum|Fe where the vacuum layer was so thick (four principal layers, corresponding to a thickness of 11.466 Å) that the LDOS corresponds closely to that of a free Fe(001) surface. The two curves, displaced vertically for clarity, are indistinguishable, illustrating the equivalence of the two Green's functions defined in (18) and (21). Moreover, the LDOS are in essential agreement with results found previously for a Fe(001) surface.[47]

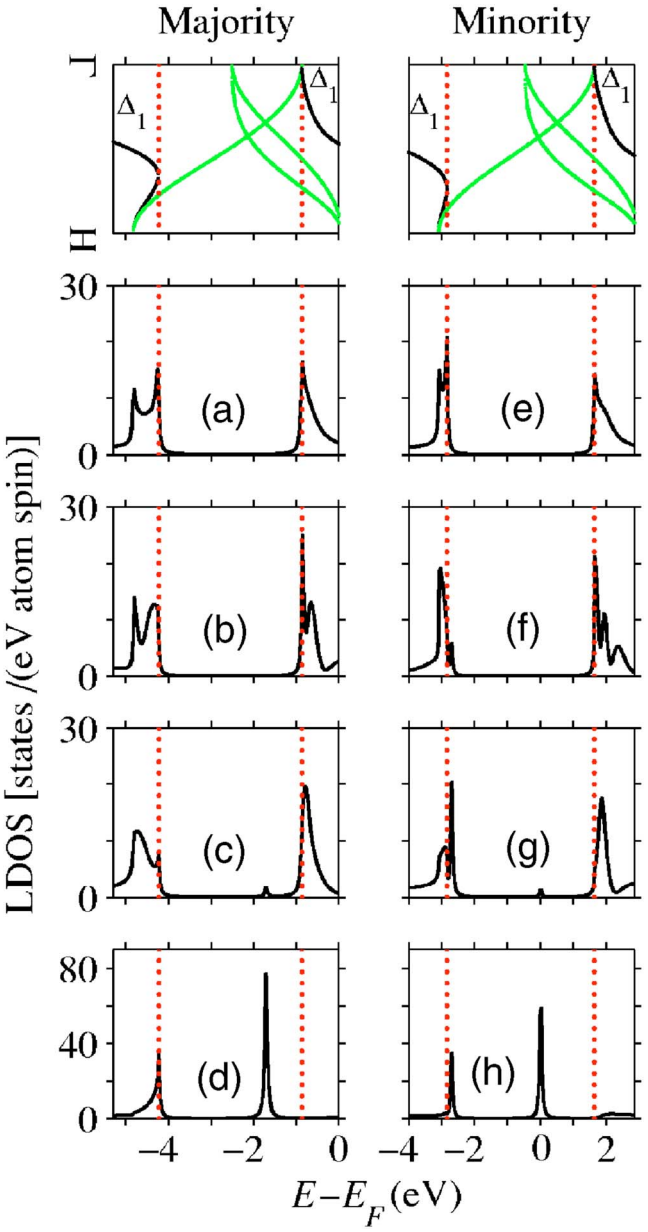

FIG. 4. (Color online) The top panels represent the band structures along Γ-H of bulk Fe for majority and minority spins. Panels (a–h) give the Δ_1 contribution to the LDOS $\rho_i(E)$ at $\bar{\Gamma}$ of the Fe|vacuum interface as a function of the layer position. (a) LDOS of an Fe layer at an infinite distance from the interface; the double-peak structure below −4 eV and single peak (of a double peak structure) above −1 eV correspond to the Δ_1 bulk bands. (b) LDOS of the 6th Fe layer (the surface layer is layer 1). (c) LDOS of the 3rd Fe layer; the sharp peak in the bulk band gap corresponds to a surface state. (d) LDOS of the the surface Fe layer; the surface-state peak has maximum amplitude. (e–h) Same for minority spin.

If one resolves the LDOS into contributions from different parts of the surface Brillouin zone, then the contribution at $\bar{\Gamma}$ ($\mathbf{k}_\parallel$=0) exhibits sharp peaks near the Fermi level. These are associated with characteristic surface states found on (001) surfaces of bcc transition metals.[48] These surface states are mainly derived from $d_{3z^2-r^2}$ orbitals on the surface atoms

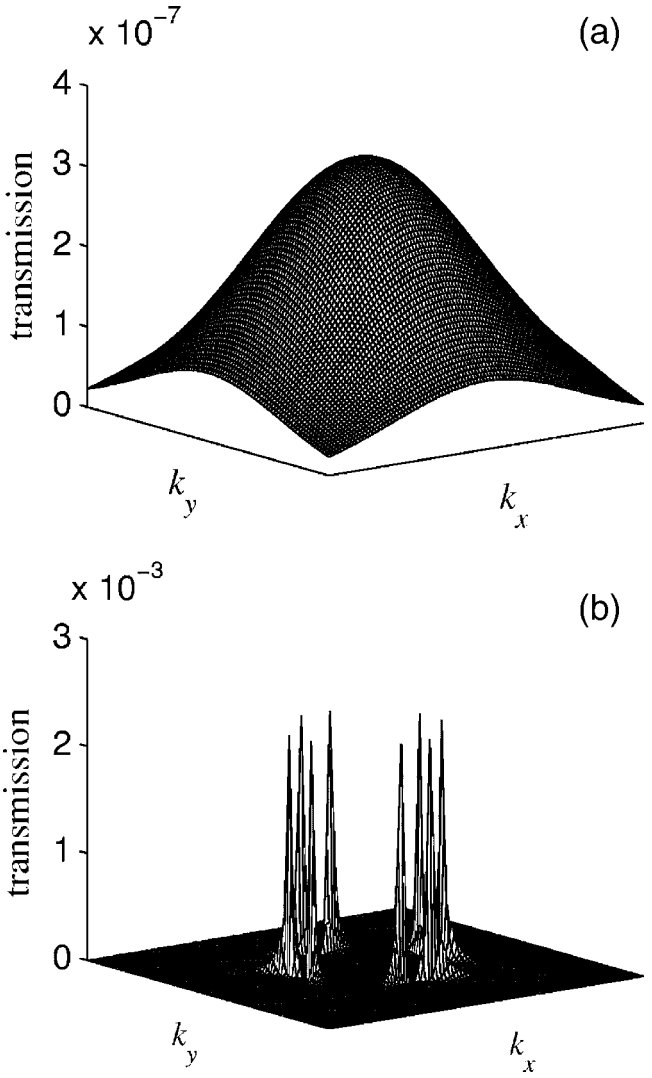

FIG. 5. Calculated $\mathbf{k}_{\|}$-resolved transmission in (a) the majority and (b) the minority spin channels through an Fe|vacuum|Fe tunnel junction. The vacuum region has a thickness of 5.733 Å and the Fe electrodes have a parallel magnetization. Only the central part of the Brillouin zone is shown, i.e., $-\pi/3a \leq k_x, k_y \leq \pi/3a$; the transmission in the other parts is close to zero.

projecting into the vacuum, and they have Δ_1 symmetry.[49,50] They become most clearly visible if one filters out the contribution to the LDOS at $\bar{\Gamma}$ of the states with Δ_1 symmetry.

This contribution, calculated using the mode-matching approach, is shown in Fig. 4 as a function of the distance from the surface. In the majority spin LDOS, a sharp peak is found at $E_F - 1.8$ eV, which is very prominent in the surface Fe layer [cf. Fig. 4(d)] and decays rapidly into the bulk [cf. Figs. 4(a)–4(c)]. This evanescent state clearly represents a state that is localized at the surface. In the minority spin LDOS, a sharp peak with similar properties is found very close to E_F. It corresponds to the surface state that is observed experimentally by a scanning tunnel microscope (STM).[48] The positions of both these surface state peaks in the majority and minority LDOS are in excellent agreement with those obtained using a Green's-function (KKR) approach.[49,50] Such surface states are good examples of evanescent states. Clearly, they are described properly within the mode-matching approach, which was, however, disputed in Ref. 22.

Using the mode-matching approach, we next calculate the transmission through an Fe|vacuum|Fe tunnel junction in which the vacuum region is only 5.733 Å thick (corresponding to two principal layers) and the magnetizations are parallel. Figure 5 shows the calculated $\mathbf{k}_{\|}$-resolved transmission for majority- and minority-spin channels. The majority conductance has a maximum at $\bar{\Gamma}$ and decreases smoothly going away from $\bar{\Gamma}$. This behavior is quite general for scattering from a potential barrier. At fixed energy, a wave traveling perpendicular to the vacuum barrier penetrates furthest into the vacuum and therefore has a maximum tunneling probability.[51]

In contrast, the minority conductance is dominated by sharp spikes of very high intensity, close to 0.13 $\overline{\Gamma X}$. This behavior has been analyzed in terms of interface resonant states that extend relatively far into the vacuum. States originating from the two Fe|vacuum interfaces couple through the thin vacuum region, which enhances the transmission considerably.[51] These transmission spikes or "hot spots" are observed quite generally in calculations for perfect transition metal|insulator|transition metal tunnel junctions.[52,53] A calculation using Eq. (30) gives the same transmission within numerical accuracy. It again illustrates the correct treatment of evanescent states within the mode-matching approach. We have also tested expression (67) numerically and found that it too gives the same transmission within numerical accuracy.

Finally, the invariance property of the transmission discussed in Sec. V C, has been tested numerically by moving the interfaces between the leads and the scattering region, where the matching is carried out, into the leads. In this way more and more slices of lead are treated as scattering region (see Fig. 1); the transmission should be invariant under this operation. Adding up to ten principal layers (20 monolayers) of bulk Fe to each side of the scattering region changes the transmission negligibly, by less than one part in 10^8.

VII. SUMMARY AND CONCLUSIONS

We have demonstrated the equivalence of the mode-matching and Green's-function approaches to calculating the conductance of quantum wires and interfaces. In the mode-matching technique, the scattering problem is solved by matching the wave function in the scattering region to the Bloch modes in the leads. The technique is formulated for tight-binding Hamiltonians and covers all representations that can be expressed in tight-binding form, including first-principles implementations using localized orbital basis sets or a real-space grid.

Alternatively, the scattering information can be extracted from the Green's function, which is calculated by partitioning the system into a scattering region and leads. We demonstrate that the Green's-function technique can be reformulated in terms of mode matching. In addition, we prove that the mode-matching expression for the transmission matrix does not depend on where in the leads the scattering region is

matched to the ideal leads, which was called into question in Ref. 22.

Calculating the full transmission matrix allows us to study individual scattering amplitudes from and to every possible mode. We have derived a compact expression for the transmission matrix elements [Eq. (67)]. Only propagating modes enter this expression, since evanescent modes do not contribute to the transmission directly. The evanescent modes are important, however, for setting up the correct matching conditions at the boundaries between the scattering region and the leads. Alternatively, the total transmission probability can be calculated from the Caroli expression [Eq. (53)]. Formally this expression sums over all possible modes, i.e., propagating and evanescent. However, by deriving the Caroli expression from the mode-matching approach we show explicitly that only the propagating modes give a nonzero contribution.

The mode-matching approach and its equivalence to the Green's-function approach were illustrated for a simple analytical model, as well as by numerical calculations on an Fe|vacuum|Fe tunnel junction. In the latter we treat the electronic structure within DFT, using a TB-MTO-ASA basis set. We demonstrate that the layer densities of states that follow from the mode-matching and Green's-function approaches are numerically indistinguishable. We identify the Fe(001) surface state in the density of states and establish its contribution to the transmission through the tunnel junction. Finally, the invariance property discussed above is demonstrated numerically on the Fe|vacuum|Fe tunnel junction.

ACKNOWLEDGMENTS

This work was financially supported by the "Nederlandse Organisatie voor Wetenschappelijk Onderzoek (NWO)" via the research programs of "Chemische Wetenschappen (CW)" and the "Stichting voor Fundamenteel Onderzoek der Materie (FOM)"; by "NanoNed," a nanotechnology program of the Dutch Ministry of Economic Affairs; by the European Commission's Research Training Network "Computational Magnetoelectronics" (Contract No. HPRN-CT-2000-00143); and by the NEDO International Joint Research program "Nano-scale Magnetoelectronics." Part of the calculations were performed with a grant of computer time from the "Stichting Nationale Computerfaciliteiten (NCF)."

APPENDIX A: VELOCITY MATRIX

In this appendix we will prove that

$$\mathbf{V}(\pm)_{m,n} = \frac{\hbar}{a} v_m(\pm)\,\delta_{m,n}, \tag{A1}$$

for the expression introduced for the velocity matrices in Sec. V D [Eq. (59)]. Here, a is the translation period along the wire and, for right-, respectively, left-propagating states, $v_n(\pm)$ is the Bloch velocity in the direction of the quantum wire. For evanescent states $v_n(\pm)=0$.

For ease of notation we drop the index $\pm$ in the following. From Eq. (4) and its complex conjugate one has

$$-\mathbf{u}_m^\dagger \mathbf{B}\mathbf{u}_n + \lambda_n \mathbf{u}_m^\dagger (E\mathbf{I}-\mathbf{H})\mathbf{u}_n - (\lambda_n)^2 \mathbf{u}_m^\dagger \mathbf{B}^\dagger \mathbf{u}_n = 0, \tag{A2a}$$

$$-\mathbf{u}_m^\dagger \mathbf{B}^\dagger \mathbf{u}_n + \lambda_m^* \mathbf{u}_m^\dagger (E\mathbf{I}-\mathbf{H})\mathbf{u}_n - (\lambda_m^*)^2 \mathbf{u}_m^\dagger \mathbf{B}\mathbf{u}_n = 0. \tag{A2b}$$

Multiplying Eq. (A2a) by λ_m^*, Eq. (A2b) by λ_n, and subtracting the two gives

$$[\lambda_n \mathbf{u}_m^\dagger \mathbf{B}^\dagger \mathbf{u}_n - \lambda_m^* \mathbf{u}_m^\dagger \mathbf{B}\mathbf{u}_n](1-\lambda_m^*\lambda_n) = 0 \Leftrightarrow -i\mathbf{V}_{m,n}(1-\lambda_m^*\lambda_n) = 0, \tag{A3}$$

according to Eq. (59). So if $\lambda_m^*\lambda_n \neq 1$ then $\mathbf{V}_{m,n}=0$.

The velocity matrices contain, by construction, either right- or left-going modes. For right-going evanescent modes one has $|\lambda|<1$, for left-going evanescent modes $|\lambda|>1$, so $\lambda_m^*\lambda_n \neq 1$ if n and/or m denotes an evanescent mode; thus $\mathbf{V}_{m,n}=0$. For propagating states, $|\lambda_m|=1$ and one can write $\lambda_m=\exp(ik_m a)$. It is obvious that if $k_m \neq k_n$, then $\lambda_m^*\lambda_n \neq 1$, and again $\mathbf{V}_{m,n}=0$.

This argument does not hold for the diagonal matrix elements of propagating states and also not for degenerate propagating states, i.e., if $\lambda_m=\lambda_n$. In the latter case we take the derivative d/dE of Eq. (A2a). The coefficients of the terms in $d\mathbf{u}_n/dE$ and $d\mathbf{u}_m^\dagger/dE$ vanish because $\mathbf{u}_n$ and $\mathbf{u}_m^\dagger$ satisfy the eigenvalue equation [Eq. (4)] and its complex conjugate, respectively, and $\lambda_n^*=1/\lambda_n$ for propagating states. Collecting the remaining terms gives

$$-\frac{d\lambda_n}{dE}[\lambda_n \mathbf{u}_m^\dagger \mathbf{B}^\dagger \mathbf{u}_n - \lambda_n^* \mathbf{u}_m^\dagger \mathbf{B}\mathbf{u}_n] + \lambda_n \mathbf{u}_m^\dagger \mathbf{u}_n = 0 \Leftrightarrow i\frac{d\lambda_n}{dE}\mathbf{V}_{m,n} + \lambda_n \mathbf{u}_m^\dagger \mathbf{u}_n = 0, \tag{A4}$$

where we emphasize that for $m \neq n$ this only holds for degenerate propagating states. Without loss of generality, degenerate states can be chosen orthogonal, i.e., $\mathbf{u}_m^\dagger \mathbf{u}_n = 0$ for $m \neq n$. Since $d\lambda_n/dE \neq 0$, it then follows that $\mathbf{V}_{m,n}=0$ if $m \neq n$.

The diagonal matrix elements $m=n$ for propagating states are also given by Eq. (A4). Setting $n=m$ and using the fact that the states are normalized (i.e., $\mathbf{u}_n^\dagger \mathbf{u}_n = 1$) gives the expression

$$\mathbf{V}_{n,n} = i\lambda_n \frac{dE}{d\lambda_n}. \tag{A5}$$

Since for propagating states we can write $\lambda_n=\exp(ika)$ and the Bloch velocity is defined as $v_n=\hbar^{-1}dE/dk$, this then proves both Eqs. (A1) and (5).

It is straightforward to derive an alternative expression for the velocity matrices in terms of the advanced matrices

$$\mathbf{V}(\pm) = i[\mathbf{U}^{a\dagger}(\mp)\mathbf{B}^\dagger \mathbf{U}^a(\mp)\mathbf{\Lambda}^a(\mp) - \mathbf{\Lambda}^{a\dagger}(\mp)\mathbf{U}^{a\dagger}(\mp)\mathbf{B}\mathbf{U}^a(\mp)]. \tag{A6}$$

Multiplying from the left by $[\mathbf{\Lambda}^{a\dagger}]^{-1}$ and from the right by $[\mathbf{\Lambda}^a]^{-1}$, this expression is seen to be equivalent to

$$\mathbf{V}(\pm) = i[\{\mathbf{\Lambda}^{a\dagger}(\mp)\}^{-1}\mathbf{U}^{a\dagger}(\mp)\mathbf{B}^\dagger \mathbf{U}^a(\mp) - \mathbf{U}^{a\dagger}(\mp)\mathbf{B}\mathbf{U}^a(\mp)\{\mathbf{\Lambda}^a(\mp)\}^{-1}]. \tag{A7}$$

APPENDIX B: PROJECTOR MATRIX

In order to prove Eq. (63), we start from Eq. (14) and rewrite it using Eq. (42) as

$$\mathbf{Q}_0 = \mathbf{B}_L \mathbf{F}_L^{-1}(+) - [\mathbf{F}_L^{a\dagger}(-)]^{-1}\mathbf{B}_L^{\dagger}. \tag{B1}$$

In the following we will drop the subscript L for ease of notation. Multiplying (B1) on the left with the identity operator $\mathbf{I}=\Sigma \mathbf{u}_n(+)\tilde{\mathbf{u}}_n^{\dagger}(+)$ and on the right with $\mathbf{I}=\Sigma \tilde{\mathbf{u}}_m^{a}(-)\mathbf{u}_m^{a\dagger}(-)$ yields

$$\mathbf{Q}_0 = \sum_{m,n=1}^{N} \tilde{\mathbf{u}}_m^{a}(-)\tilde{\mathbf{u}}_n^{\dagger}(+)\left[\frac{1}{\lambda_n(+)}\mathbf{u}_m^{a\dagger}(-)\mathbf{B}\mathbf{u}_n(+) - \frac{1}{\lambda_m^{a*}(-)}\mathbf{u}_m^{a\dagger}(-)\mathbf{B}^{\dagger}\mathbf{u}_n(+)\right], \tag{B2}$$

where use has been made of Eqs. (6), (7), and (36).

By similar arguments as those leading to Eq. (A3), it follows that $[\ldots]=0$, unless $\lambda_m^a(-)=1/\lambda_n^*(+)$. From Eq. (36) it follows that this is true if $n=m$ and n denotes a propagating mode. In addition, for every $(+)$ evanescent mode n with eigenvalue $\lambda_n(+)$, there is one $(-)$ evanescent mode with eigenvalue $\lambda_n(-)=1/\lambda_n^*(+)$.[31] Again it follows from Eq. (36) that only the $m=n$ terms are nonzero for evanescent modes in Eq. (B2). This equation then simplifies to

$$\begin{aligned}\mathbf{Q}_0 = &\sum_{n=1}^{N_p} \tilde{\mathbf{u}}_n^{a}(-)\tilde{\mathbf{u}}_n^{\dagger}(+) \times\left[\frac{1}{\lambda_n(+)}\mathbf{u}_n^{\dagger}(+)\mathbf{B}\mathbf{u}_n(+) - \lambda_n(+)\mathbf{u}_n^{\dagger}(+)\mathbf{B}^{\dagger}\mathbf{u}_n(+)\right] \\ &+ \sum_{n=N_p+1}^{N} \tilde{\mathbf{u}}_n^{a}(-)\tilde{\mathbf{u}}_n^{\dagger}(+) \times\left[\frac{1}{\lambda_n(+)}\mathbf{u}_n^{\dagger}(-)\mathbf{B}\mathbf{u}_n(+) - \lambda_n(+)\mathbf{u}_n^{\dagger}(-)\mathbf{B}^{\dagger}\mathbf{u}_n(+)\right],\end{aligned} \tag{B3}$$

where the first summation is over the N_p propagating modes and the second summation is over the $N-N_p$ evanescent modes.

The projector matrix $\mathbf{P}$ is defined by Eq. (62). In the product $\mathbf{Q}_0\mathbf{P}$ only the first summation in Eq. (B3) survives. Moreover, since $[\ldots]=i\mathbf{V}_{n,n}$ according to Eq. (A3), we have

$$\mathbf{Q}_0\mathbf{P} = i\sum_{n=1}^{N_p} \tilde{\mathbf{u}}_n^{a}(-)\tilde{\mathbf{u}}_n^{a\dagger}(-)\mathbf{V}_{n,n}(+). \tag{B4}$$

Together with Eq. (61) this then proves Eq. (63).

*Corresponding author. E-mail address: g.brocks@tnw.utwente.nl

[1] M. N. Baibich, J. M. Broto, A. Fert, F. Nguyen van Dau, F. Petroff, P. Etienne, G. Creuzet, A. Friedrich, and J. Chazelas, Phys. Rev. Lett. **61**, 2472 (1988).

[2] G. Binasch, P. Grünberg, F. Saurenbach, and W. Zinn, Phys. Rev. B **39**, 4828 (1989).

[3] N. Agraït, A. L. Yeyati, and J. M. van Ruitenbeek, Phys. Rep. **377**, 81 (2003).

[4] M. Büttiker, Y. Imry, R. Landauer, and S. Pinhas, Phys. Rev. B **31**, 6207 (1985).

[5] K. M. Schep, J. B. A. N. van Hoof, P. J. Kelly, G. E. W. Bauer, and J. E. Inglesfield, Phys. Rev. B **56**, 10805 (1997).

[6] J. B. A. N. van Hoof, K. M. Schep, A. Brataas, G. E. W. Bauer, and P. J. Kelly, Phys. Rev. B **59**, 138 (1999).

[7] J. Kudrnovský, V. Drchal, C. Blaas, P. Weinberger, I. Turek, and P. Bruno, Phys. Rev. B **62**, 15084 (2000).

[8] K. Xia, P. J. Kelly, G. E. W. Bauer, I. Turek, J. Kudrnovský, and V. Drchal, Phys. Rev. B **63**, 064407 (2001).

[9] I. Riedel, P. Zahn, and I. Mertig, Phys. Rev. B **63**, 195403 (2001).

[10] J. Taylor, H. Guo, and J. Wang, Phys. Rev. B **63**, 245407 (2001).

[11] M. Brandbyge, J. L. Mozos, P. Ordejón, J. Taylor, and K. Stokbro, Phys. Rev. B **65**, 165401 (2002).

[12] D. Wortmann, H. Ishida, and S. Blügel, Phys. Rev. B **66**, 075113 (2002).

[13] K. S. Thygesen, M. V. Bollinger, and K. W. Jacobsen, Phys. Rev. B **67**, 115404 (2003).

[14] P. Mavropoulos, N. Papanikolaou, and P. H. Dederichs, Phys. Rev. B **69**, 125104 (2004).

[15] C. Caroli, R. Combescot, P. Nozières, and D. Saint-James, J. Phys. C **4**, 916 (1971).

[16] S. Datta, *Electronic Transport in Mesoscopic Systems* (Cambridge University Press, Cambridge, England, 1995).

[17] T. Ando, Phys. Rev. B **44**, 8017 (1991).

[18] K. Nikolić and A. MacKinnon, Phys. Rev. B **50**, 11008 (1994).

[19] K. Xia, P. J. Kelly, G. E. W. Bauer, A. Brataas, and I. Turek, Phys. Rev. B **65**, 220401(R) (2002).

[20] K. Xia, P. J. Kelly, G. E. W. Bauer, and I. Turek, Phys. Rev. Lett. **89**, 166603 (2002).

[21] M. Zwierzycki, K. Xia, P. J. Kelly, G. E. W. Bauer, and I. Turek, Phys. Rev. B **67**, 092401 (2003).

[22] P. S. Krstić, X.-G. Zhang, and W. H. Butler, Phys. Rev. B **66**, 205319 (2002).

[23] P. Sautet and C. Joachim, Phys. Rev. B **38**, 12238 (1988).

[24] We restrict ourselves to a representation on orthogonal basis sets, but the extension to nonorthogonal basis sets is straightforward.

[25] K. Xia, M. Zwierzycki, M. Talanana, P. J. Kelly, and G. E. W. Bauer (to be published).

[26] P. A. Khomyakov and G. Brocks, Phys. Rev. B **70**, 195402 (2004).

[27] A. MacKinnon, Z. Phys. B: Condens. Matter **59**, 385 (1985).

[28] In some representations the hopping matrices can be singular. In all cases where the inverse of such a matrix would be needed, one can use the well-defined pseudoinverse matrix instead, cf. Ref. 30.

[29] F. Tisseur and K. Meerbergen, SIAM Rev. **43**, 235 (2001).

[30] G. Golub and C. F. van Loan, *Matrix Computations* (Johns Hopkins University Press, Baltimore, 1996).

[31] L. Molinari, J. Phys. A **30**, 983 (1997).

[32] The current per mode is given by velocity times density. Since we normalize a mode in a slice, its density is given by 1/thickness of the slice.
[33] E. Godfrin, J. Phys.: Condens. Matter **3**, 7843 (1991).
[34] A. R. Williams, P. J. Feibelman, and N. D. Lang, Phys. Rev. B **26**, 5433 (1982).
[35] I. Turek, V. Drchal, J. Kudrnovský, M. Šob, and P. Weinberger, *Electronic Structure of Disordered Alloys, Surfaces and Interfaces* (Kluwer, Dordrecht, 1997).
[36] F. Guinea, C. Tejedor, F. Flores, and E. Louis, Phys. Rev. B **28**, 4397 (1983).
[37] D. S. Fisher and P. A. Lee, Phys. Rev. B **23**, R6851 (1981).
[38] A. Messiah, *Quantum Mechanics* (North-Holland, Amsterdam, 1961).
[39] S. Sanvito, C. J. Lambert, J. H. Jefferson, and A. M. Bratkovsky, Phys. Rev. B **59**, 11936 (1999).
[40] A. Umerski, Phys. Rev. B **55**, 5266 (1997).
[41] P. A. Khomyakov (unpublished).
[42] T. Kostyrko, Phys. Rev. B **62**, 2458 (2000).
[43] H. U. Baranger and A. D. Stone, Phys. Rev. B **40**, 8169 (1989).
[44] L. D. Landau and E. M. Lifschitz, *Quantum Mechanics: Non-relativistic Theory* (Pergamon Press, Oxford, 1981), §128.
[45] J. P. Perdew and A. Zunger, Phys. Rev. B **23**, 5048 (1981).
[46] O. K. Andersen, O. Jepsen, and D. Glötzel, in *Highlights of Condensed Matter Theory*, edited by F. Bassani, F. Fumi and M. P. Tosi (North-Holland, Amsterdam, 1985), pp. 59–176.
[47] C. S. Wang and A. J. Freeman, Phys. Rev. B **24**, 4364 (1981).
[48] J. A. Stroscio, D. T. Pierce, A. Davies, R. J. Celotta, and M. Weinert, Phys. Rev. Lett. **75**, 2960 (1995).
[49] C. Uiberacker and P. M. Levy, Phys. Rev. B **64**, 193404 (2001).
[50] C. Uiberacker and P. M. Levy, Phys. Rev. B **65**, 169904(E) (2002).
[51] O. Wunnicke, N. Papanikolaou, R. Zeller, P. H. Dederichs, V. Drchal, and J. Kudrnovský, Phys. Rev. B **65**, 064425 (2002).
[52] W. H. Butler, X.-G. Zhang, T. C. Schulthess, and J. M. MacLaren, Phys. Rev. B **63**, 054416 (2001).
[53] J. Mathon and A. Umerski, Phys. Rev. B **63**, 220403(R) (2001).